Temperature Effect Analysis of PVDF-Based Piezoelectric Energy Harvester

Chandana Ravikumar, Vytautas Markevičius, Dangirutis Navikas, Mindaugas Čepėnas, Algimantas Valinevičius, Mindaugas Žilys, Roman Šotner, *Member, IEEE*, Jan Jerabek, Zhixiong Li, *Senior Member, IEEE*, Jan Včelák, Darius Andriukaitis*, *Member, IEEE*

Abstract—This study presents a comprehensive investigation into the temperature-dependent performance of polyvinylidene fluoride (PVDF)-based piezoelectric energy harvesters (PEHs), integrating both experimental analysis and finite element modeling. The primary objective is to elucidate the influence of temperature variations on the electrical output and resonant frequency of PVDF-based PEHs, thereby enhancing the reliability and efficiency of energy harvesting systems in diverse thermal environments. Recognizing that environmental conditions play a significant role in the degradation and failure of electronic devices, this research evaluates the electrical output and resonant frequency of PEHs across a temperature range of –20 °C to 50 °C. Four identical PEH prototypes were fabricated and subjected to controlled temperature conditions, revealing a nonlinear increase in output voltage and power with rising temperature, while the resonant frequency remained relatively stable.

A new, flexible test rig was set up to easily check how PEH devices perform in different temperatures, and it can also be scaled up for testing many devices in large production. To accurately simulate the observed behavior, finite element models incorporating experimentally derived Rayleigh damping coefficients were developed using COMSOL Multiphysics. The simulations closely matched the experimental data, validating the effectiveness of the damping parameters in capturing the dynamic response of the PEHs under varying thermal conditions. The proposed methodology provides a strong basis for future research into thermal aging effects, long-term durability, and performance optimization of polymer-based energy harvesters. The findings underscore the suitability of PVDF as a piezoelectric material with a steel substrate for energy harvesting applications.

Index Terms—Finite element modelling, Piezoelectric material, Renewable energy harvesting, Rayleigh Damping, Reliability, Sustainable IoT, Thermal effect.

I. Introduction

Piezoelectric vibration energy harvesting (PVEH) has emerged as a promising alternative to conventional batteries for powering ultra-low-power IoT and embedded systems. Prior studies have shown that optimized energy harvesters can deliver sustained power for over 10 years, potentially tripling device lifespan and significantly reducing maintenance through self-sustained operation. In this paper we demonstrate the concept of using a piezoelectric bimorph beam for energy harvesting based on vertical vibrational motion. Vibration at a particular frequency causes piezoelectric beam plucking and subsequently output voltage will be generated as a result of the deformation of the piezoelectric beam.

Temperature affects several key material properties of Polyvinylidene difluoride (PVDF), which in turn influence harvester behavior. The PVDF's piezoelectric coefficient d33 gradually changes with temperature. Generally, heating causes a slight decrease in piezoelectric coefficients due to increased dipole randomness (thermal agitation) for example, one study found PVDF's d33 drops linearly from about –17 pC/N at 25 °C down to –6.5 pC/N by 130 °C [1]. At low temperatures, conversely, dipoles are more stably aligned, so PVDF can exhibit slightly higher piezoelectric response when cooled (fewer thermal disruptions) [2].

Manuscript received 20 May 2023 (Corresponding author: Darius Andriukaitis).

Chandana Ravikumar, Vytautas Markevičius, Dangirutis Navikas, Mindaugas Čepėnas, Algimantas Valinevičius, Mindaugas Žilys, and Darius Andriukaitis are with the Department of Electronics Engineering, Kaunas University of Technology, Kaunas, Lithuania (emails: chandana.ravikumar@ktu.edu, vytautas.markevicius@ktu.lt, dangirutis.navikas@ktu.lt, mindaugas.cepenas@ktu.lt, algimantas.valinevicius@ktu.lt, mindaugas.zilys@ktu.lt, darius.andriukaitis@ktu.lt).

Chandana Ravikumar is with the department of Physics of materials in Charles University, Prague, Czech Republic (e-mail: chandana.ravikumar@matfyz.cuni.cz)

Jan Vcelek is with the Department Electronic Systems and Diagnostics research team, University Center for Energy Efficient Buildings, Czech Technical University in Prague, Czech Republic (e-mail: jan.vcelak@cvut.cz)

Roman Sotner is with the Department of Radio Electronics, Faculty of Electrical Engineering and Communication, Brno University of Technology, Brno, Czech Republic (e-mail: sotner@vutbr.cz).

Jan Jerabek is with the Department of Telecommunications, Faculty of Electrical Engineering and Communication, Brno University of Technology, Brno, Czech Republic (e-mail: jerabekj@feec.vutbr.cz).

Zhixiong Li is with the Faculty of Mechanical Engineering, Opole University of Technology, Opole, Poland (e-mail: zhixiong.li@ieee.org).

It is crucial to test the PVDF-based piezoelectric energy harvesters in the temperature spans that cover typical environmental conditions while staying within the polymer's stable operating limits. PVDF's glass transition is around –35 °C and melting point ~170 °C [3], so –20 °C to +50 °C avoids the extremes of brittleness or permanent polarization loss. In this range, PVDF (polyvinylidene fluoride) remains in its piezoelectric β-phase with no phase transitions or depoling. Moreover, many researchers [4] use this range to simulate real-world climates (winter cold to summer heat) for IoT sensors and devices. Staying in this band ensures the harvester's materials (PVDF film, any substrates or adhesives) operate without irreversible changes, focusing only on the reversible effects of temperature on performance.

There is a lack of an integrated experimental and simulation-based analysis that spans this full temperature range. Analytical modeling approaches, including Euler–Bernoulli and Timoshenko beam theory, have been used to evaluate cantilever-type PVEHs [5], [6] but their applicability is limited by assumptions of linearity and simplified geometries. In contrast, finite element modeling (FEM) allows the simulation of complex coupled thermo-mechanical-electrical behavior, accounting for nonlinear variations in PVDF's piezoelectric and elastic properties with temperature. Commercial tools like COMSOL support temperature-dependent material parameters and enable full 3D modeling of multilayer structures including adhesive layers and proof masses.

Despite this, accurate damping modeling remains a critical gap. While the loss factor method is often used to represent material damping in the frequency domain, studies have shown it can overestimate output by up to 50% compared to experimental results [7] [8] Rayleigh damping, calibrated using experimentally derived modal damping ratios, provides a more physically representative model of system-wide energy dissipation and is crucial for dynamic simulations [9]

Experimental validation is equally limited by the availability of adaptable test benches. Standardized rigs are impractical due to the diverse designs of PVEH systems. As a result, researchers often develop custom test rigs to accommodate real-time parameter changes and accurately capture temperature-variant responses [10]. Yet, integrated efforts combining flexible test setups, measured damping coefficients, and temperature-controlled simulations are rare.

This study addresses these gaps by:

- Proposing a novel PVDF-based PVEH optimized for vertical vibration harvesting.
- Developing a 3D FEM model with experimentally calibrated Rayleigh damping coefficients.
- Simulating device behavior across −20 °C to 50 °C, and validating against four physical prototypes tested in a controlled thermal environment.
- Designing a modular experimental test bench for in situ electrical and mechanical characterization.

Through this combined modeling and experimental approach, the work provides a realistic and temperature-resilient performance assessment of PVEHs, offering new insight into long-term deployment under variable environmental conditions. The overview of this study is shown in Figure 1.

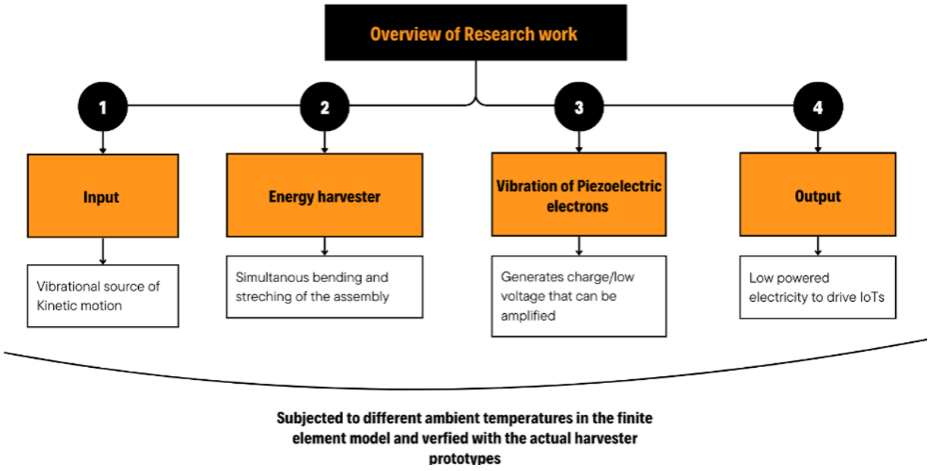

Fig. 1. An overview of the research paper.

The remainder of the paper is presented in the following order. Section II presents the summary of related works. Section III introduces the overall design of our proposed model, where detailed steps are presented with the designs. Section IV shows the Rayliegh damping experiments. Section V explains the finite element model prepared and Section VI analyses the performance of the model system against various temperature conditions. Section VII presents the practical experiment setup and displays the experiment evaluation results alongside simulation results. Section VIII presents a detailed discussion of the results along with a comparative analysis against existing studies, while Section IX provides a concise summary of the key conclusions drawn from this work.

II. RELATED EXISTING WORKS

Polyvinylidene fluoride (PVDF) is widely used in piezoelectric energy harvesters (PVEHs) due to its flexibility and electroactive properties. However, its performance is highly sensitive to environmental factors. Studies have shown that PVDF exhibits thermal instability, with degradation accelerated by high temperatures and UV exposure [8],[9],[10]. Mechanical testing at room and sub-zero temperatures has

revealed significant dependencies on both strain rate and temperature [11],[12] Notably, under high-stress conditions, the glass transition temperature of PVDF shifts closer to 0 °C [13], [14], indicating reduced mechanical resilience in cold environments. Despite these insights, existing literature lacks an integrated simulation–experiment framework to quantify how these thermal effects influence the mechanical and electrical behavior of PVDF-based cantilever harvesters [15], [16].

Furthermore, most experimental studies rely on fixed test configurations that limit the adaptability needed for temperature-variant testing. For example, the system in [17] shown in Figure 2(a) simulates human gait energy harvesting using a fixed 1 Hz sinusoidal excitation (6.3 g), which fails to represent the natural frequency range of human motion (0.5–2.5 Hz) and uses analog accelerometers prone to drift. Similarly, [18] presents a rotor-based excitation mechanism that enables delayed actuation but suffers from inconsistent inputs and low-resolution voltage tracking via a digital multimeter seen in Figure 2(b).

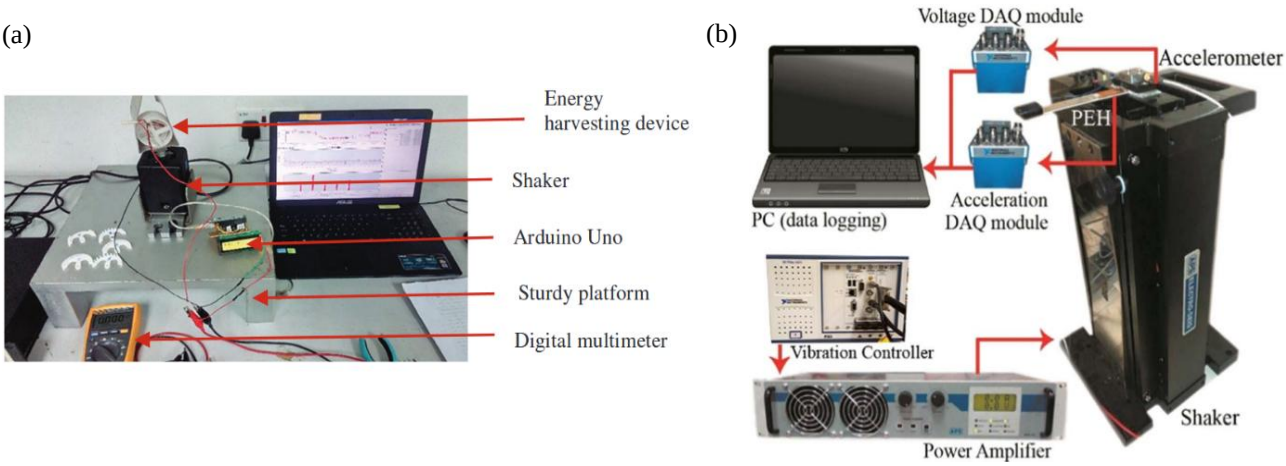

Fig. 2. (a) Human gait energy harvesting test setup[17]; (b) Experimental setup to measure output voltage of rotational piezoelectric harvester [18]

Another critical limitation in prior models is the insufficient incorporation of realistic damping [19], [20]. While Rayleigh damping is a standard practice in finite element modeling (FEM), few studies calibrate its coefficients experimentally. This compromises model accuracy when simulating energy dissipation in multilayer structures. Our study addresses this gap by experimentally deriving Rayleigh damping coefficients from two eigenfrequencies and incorporating them into a 3D FEM simulation in COMSOL, yielding improved alignment with physical test results. This work contributes a unified investigation by developing a reconfigurable test rig, performing multi-temperature tests on PVDF–steel cantilevers, and validating simulation results using experimentally determined damping parameters - thus enabling a more accurate and holistic assessment of energy harvester performance under real-world thermal conditions.

III. Dimensions of the Piezoelectric Beam

Harvesting energy using a piezoelectric cantilever with proof mass requires precise selection of beam geometry and material properties to optimize voltage output. In this study, simulations were performed in COMSOL Multiphysics® to evaluate the performance of a bimorph cantilever beam composed of two PVDF layers (each 14 mm × 64 mm × 0.03 mm), separated by a copper electrode, and fixed to a steel substrate (23 mm × 64 mm × 0.1 mm). The cantilever is clamped at one end (3 mm × 3 mm × 3 mm) and attached to a proof mass (14 mm × 64 mm × 2.65 mm) weighing 29 g, as seen in Figure 3.

PVDF was selected due to its mechanical flexibility and favorable piezoelectric coefficient ($d_{31} = 25$ pC/N), Young's modulus ($E = 2500$ MPa), and relative permittivity ($\varepsilon/\varepsilon_0 = 9.5$). The simulations accounted for material damping using experimentally derived Rayleigh coefficients ($\alpha_1 = 0.51$, $\alpha_2 = 1.04\times10^{-6}$). In piezoelectric energy harvesting systems, the optimal load resistance is known to be influenced by factors such as excitation frequency, mechanical damping, and notably, temperature [22]-[28]. However, in the context of this study, the choice to use a fixed load resistance was a deliberate decision aimed at isolating and analyzing the specific effects of temperature on the energy harvester's performance. The harvester was modeled under 1 g sinusoidal excitation at low frequency with a load resistance of 310 kΩ selected as the optimum load.

To establish the constant load, the authors first performed a bench-top sweep of external resistance from 10 kΩ to 2 MΩ at 25 °C; the harvested power peaked sharply at 310 kΩ, which therefore represents the maximum-power-transfer point for the device's intrinsic source impedance and fixed this value for all subsequent temperature runs. Although a full sweep at every temperature could marginally refine the match, our goal in this materials-focused study was to isolate the temperature response of the PVDF transducer under a constant, well-defined load. A single resistance eliminates an extra degree of freedom, ensuring that any power change reflects the device—not a re-tuned interface. Finite-element modelling with temperature-dependent material constants indicates the source impedance drifts by <10 % between 0 °C and 80 °C, keeping the chosen 310 kΩ within the flat-top region of the power-versus-load curve where efficiency varies by less than 5 %. Therefore, considering one sweep is sufficient for the objectives of this work. That said, the authors acknowledge that adaptive impedance-matching techniques [23](e.g., MPPT or SSHI

circuits) could capture the residual mismatch losses, and plan to incorporate a programmable-load rig and adaptive interface in future studies to quantify these additional gains.

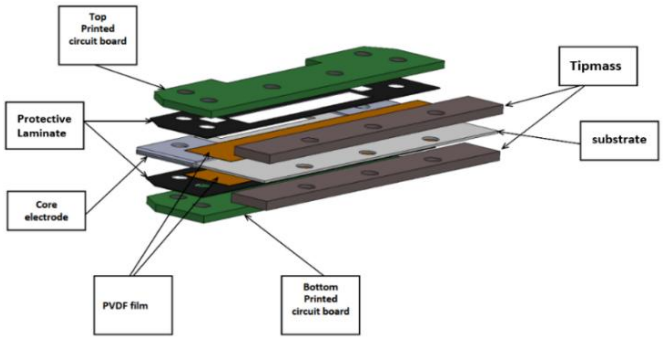

Fig. 3. The constituent structure of proposed piezoelectric energy harvester

IV. Modeling Piezoelectric Energy Harvester

The schematic diagram is shown in Fig. 4(b). The major parameters mentioned as global definitions in COMSOL Multiphysics simulation software are listed in Table 1. This table provides a comprehensive set of material, damping, and geometric parameters crucial for analyzing and modeling the performance of the PVDF-based piezoelectric cantilever. The study on the Rayliegh damping experimental values in given in the appendix.A 3D FEM as per the design parameters mentioned above is constructed, depicted in Fig. 4(a). The parallel connection between the two metalized (thin yellow layers) PVDF (grey layers) and epoxy glue (blue layers) is shown in Fig. 4(b).

The flowchart in Fig 4(c) shows the simulation procedure used in this study. Due to the extremely small thickness of the electrodes compared to the overall thickness of the EH, the mechanical effects of the electrodes have not been evaluated. It is presumed that there is perfect coupling among the steel substrate, and two layers of piezoelectric material and that there is a uniform difference in electric potential given to ideally conductive electrodes [29]. The steel core and the thin Al electrode on the surface of 30 µm PVDF film are used, bonded in the same polling and stretching directions. The metal substrate and proof mass are made of structural steel. A vertical or volumetric displacement of a volumetric load described as a kinematic excitation is applied to the EH. With this, active piezo layers are implemented, and a voltage signal is generated. Solid mechanics, electrostatics, and electrical circuits along with frequency domain study are performed in COMSOL. This model facilitates complex evaluation of cantilever response, frequency response, and electrical response to the influence of different temperatures. The lumped parameter mathematical model adopted in our study is from reference [30],

$$v(t) = -\frac{-jR\theta m_e\omega^3 Y_0 e^{j\omega t}}{({\omega_{nL}}^2-\omega^2+j2\zeta m_e\omega)\times(m_e+jm_eRC_p\omega)+jR\theta^2\omega}, \quad (1)$$

where θ is the electromechanical coupling factor, R is the load resistance, m_e is the effective mass of the beam, m_e is the effective mass of the beam, ζ is the mechanical damping ratio and C_p is the equivalent capacitance. For parallel connections of the piezoelectric layers as seen in Fig. 4(b), the equation for electromechanical coupling factor θ and equivalent capacitance $C_p$is given in reference [21].

$$\theta = \frac{2\,\mathrm{d}_{31}h_{ps}(kbL^2)}{2I}, \quad (2)$$

$$C_p = \frac{2\varepsilon_{33}^S(bL)}{h_p}, \quad (3)$$

$$h_{ps} = \frac{h_s+h_p}{2}. \quad (4)$$

So h_p and h_s are the thickness of piezoelectric layers and substrate respectively, ε_{33}^S is the permittivity strain constant, b is the width of the beam and $\mathrm{d}_{31}$is the transverse coefficient of piezoelectricity. This compressive mathematical model is simple but also considers the effect of mechanical damping on the output voltage. The proof mass attached to the cantilever is much larger than the mass of a cantilevered beam and this effect is included in the above equation. The temperature-dependent parameters of the cantilever namely poisson's ratio (ν), Young's modulus (E), and thermal coefficient value (K) change concerning time [31].

TABLE I
Geometric Values And Parameters Of The Energy Harvester Model

Piezoelectric material: PVDF (JINZHOUKEXIN Co. Ltd)		
Parameters of PVDF	**Symbols**	**Values**
Coefficient of Piezoelectricity (pC/N)	d_{31}	25
Thickness(µm)	t_b	30
Young's modulus (MPa/psi)	E	2500
Density (kg/m^3)	ρ_b	1780
Relative permittivity	$\varepsilon/\varepsilon_0$	9.5

Cantilever Rayleigh damping coefficients from measurements		
Mass coefficient (s^{-1})	α_1	0,51
Stiffness coefficient (s)	α_2	1,04E-06
Geometric values		
Steel Dimension (mm)	$L_e \times W_b \times t_s$	$23 \times 64 \times 0.1$
Single PVDF layer Dimension (mm)	$L_e \times W_b \times t_b$	$14\times 64 \times 0.03$
Fixed end Dimension (mm)	$L_m \times W_m \times t_m$	$3\times 3 \times 3$
Proof mass Dimension(mm)	$L_m \times W_m \times t_m$	$14\times 64 \times 2.65$
Weight of mass(g)	M	29
Gaps(mm)	L	10

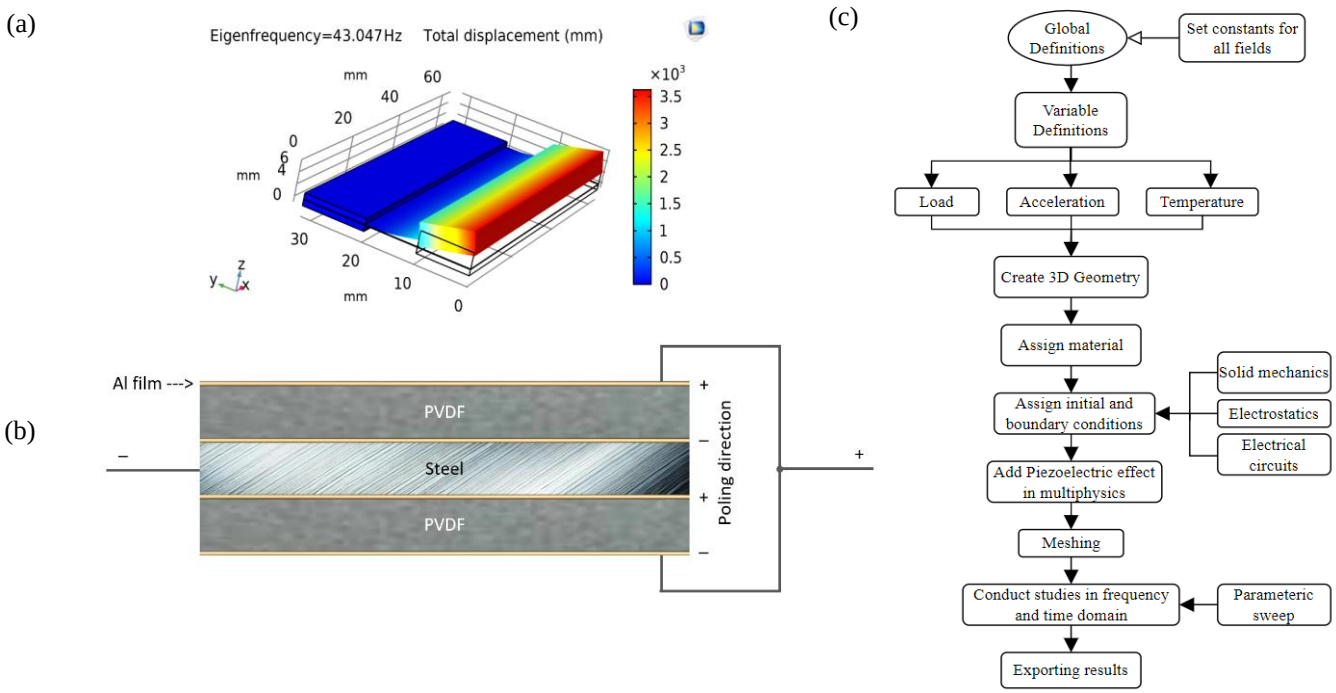

Fig. 4. (a) COMSOL finite models in 3D view showing 3 mm displacement for 0.5 g acceleration; (b) PVDF top and bottom Al metallization layers parallel connection; (c) Implementation of the temperature test procedure in COMSOL.

V. Simulation Implementation

The FEM simulation models a vertically applied sinusoidal acceleration load of 0.5g, with temperature conditions varying between −20 °C and 50 °C in 10 °C steps. Using COMSOL Multiphysics, the process begins with defining global constants and variables such as load, acceleration, and temperature. The piezoelectric effect is incorporated through Multiphysics coupling. A parametric sweep is applied to automate simulations over the 8 defined temperatures, allowing for efficient exploration of how output RMS voltage and resonant frequency change with temperature (Table 2). The system is then meshed, studied in both frequency and time domains, and results are exported for analysis.

VI. Relationship Between Temperature and Output Voltage and Resonant Frequency

Polymer-based PVDF (Polyvinylidene difluoride) material, thin metal plate, and tip mass made of structural steel and epoxy resin adhesive layers are the constituent materials used in the PVEH.

TABLE II

Calculated Temperature Coefficient of Resonant Frequency, Output RMS Voltage, and Generated Power

Sl.No	Frequency (V)		Voltage (V)		Power (μW)	
Temperature	Model	Real Avg	Model	Real Avg l	Model	Real Avg
-20^0C	43.00	41.65	9.91	8.58	329.00	246.39
-10^0C	42.98	41.75	11.167	9.09	413.29	276.23
0^0C	42.97	41.79	12.221	10.76	492.89	387.17
10^0C	42.95	41.80	13.043	12.05	562.76	485.74
20^0C	42.92	41.68	13.632	12.23	619.21	499.42
30^0C	42.91	41.57	14.019	12.55	662.07	526.06
40^0C	42.89	41.35	14.233	12.73	691.70	540.35
50^0C	42.87	41.12	14.322	13.36	710.14	596.40

As a result, they can have different temperature dependences.There is most likely a “bimaterial” effect due to differences between their thermal dilation coefficients. The temperature-dependent parameters of the cantilever namely Poisson’s ratio (ν)and Young’s modulus (E) change with

respect to time according to the equation below [31].

$$\nu = 0 \cdot 3 \times (1 + 1 \times 10^{-4}) \times T \quad (5)$$

$$E = 200 \times (1 - 3 \cdot 34 \times 10^{-4}) \times T \quad (6)$$

Where T is the temperature of the object under consideration. According to each test temperature the combined value of Poisson's ratio (ν)and Young's modulus (E) is calculated by COMSOL with the help of the above expressions and consequently, it results in a change in thermal expansion, resonant frequency, and output voltage generation.

Table 3 captures the precise values of ν and E at each test temperature, forming the foundation of the temperature-coupled simulation model. These values directly influence:

- Resonant frequency: A softer cantilever (due to reduced E) leads to a shift in the resonant frequency, as verified in the experimental-simulation comparison.
- Output voltage: Changes in mechanical compliance alter the strain distribution in the PVDF layer, thereby affecting charge generation (Figure 4(b)).
- Thermal expansion mismatch: The bimaterial interface introduces curvature or stress asymmetry, further modulating electrical performance.

Quantitatively, over the span from –20°C to 50°C:

- Poisson's ratio increases from ~0.294 to ~0.311 (Δν ≈ +5.7%), indicating slightly more lateral deformation under axial strain.
- Young's modulus decreases from ~201.34 GPa to ~186.56 GPa (ΔE ≈ –7.35%), reducing the structural stiffness of the cantilever.

In particular, the Poisson's ratio (ν) and Young's modulus (E)—two critical elastic parameters that govern the mechanical stiffness and strain distribution in the cantilever—are inherently temperature-dependent. The table quantifies these parameters over the investigated temperature range (–20°C to 50°C) using the following empirically derived equations:

TABLE III
TEMPERATURE-DEPENDENT VARIATION OF POISSON'S RATIO AND YOUNG'S MODULUS FOR THE PVEH COMPOSITE CANTILEVER

Temp (°C)	Young's modulus (GPa)	Thermal expansion (um/K)
-20	200.72	-1315.95
-10	200.54	-438.65
0	200.36	-438.65
10	200.18	-438.65
20	200	10
30	199.82	438.65
40	199.64	438.65
50	199.46	438.65

VII. PRACTICAL TEMPERATURE EXPERIMENTS

To validate the simulation results, thermal vibration tests were conducted on four nearly identical piezoelectric energy harvester prototypes. Real photographs of the lab setup, prototypes and flowchart of experiment are shown in Fig. 5(a) and 5(b). Each prototype was mounted with an electromagnetic exciter inside a temperature chamber to simulate realistic working conditions. Tests were carried out over a temperature range from −20 °C to 50 °C in 10 °C increments. At each temperature, the devices were subjected to 0.5 g sinusoidal vibrations under a fixed load resistance of 310 kΩ. Output RMS voltage and resonant frequency were recorded.

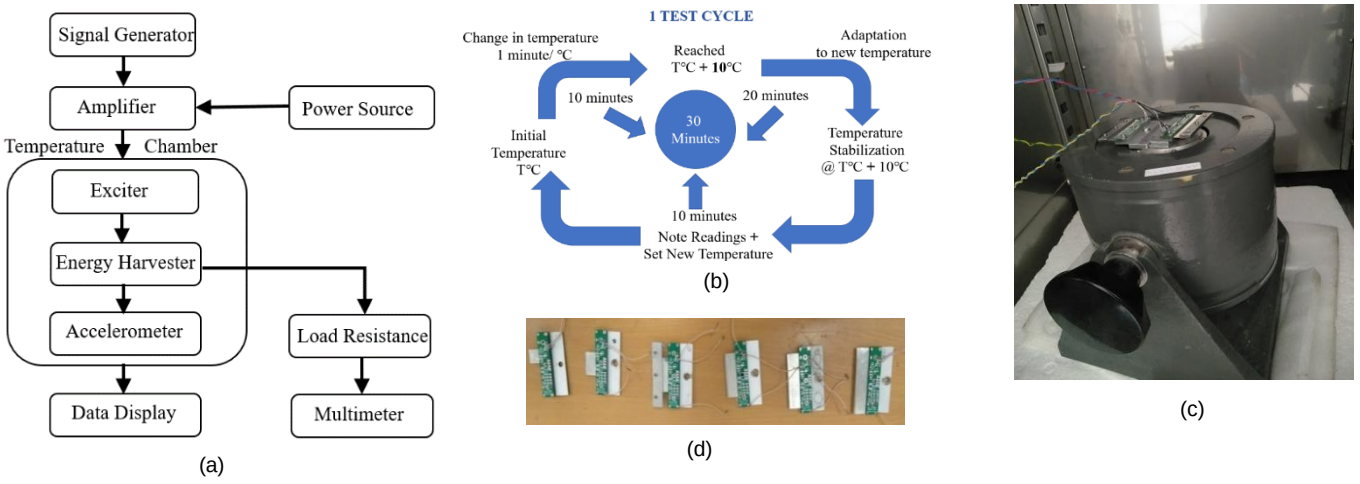

Fig. 5. (a) Flow chart of experiment setup; (b) Flow chart of single temperature test cycle; (c) Photo of energy harvester prototype (d) Prototype samples used in the experiments.

As illustrated in the test cycle diagram, each 10 °C temperature step lasted 20 minutes: 5 minutes for temperature ramp-up, 20 minutes for stabilization, and 5 minutes for measurement and resetting. Each prototype underwent 5 hours of vibration across 8 temperature points, totaling 20 hours of testing as shown in Fig 5(b). Signal I/O circuitry remained outside the chamber at ambient conditions. A temperature test chamber from Guangdong Yuanyao Test Equipment Co., Ltd was employed.

The experimental results are plotted alongside simulation data in Fig. 6, illustrating RMS voltage, resonant frequency, and generated power as functions of temperature under a uniform base excitation of 0.5g. All prototypes exhibit resonant frequencies in the range of 39–43 Hz, as shown in Fig. 6f(a). The observed variation among samples is attributed to slight differences in the manual assembly process—particularly the

tip mass gap—which can affect resonance despite identical cantilever dimensions and masses. Simulated resonant frequency values remain nearly constant across the full temperature range, from 43.00 Hz at -20 °C to 42.87 Hz at 50 °C. Experimental results similarly show minimal variation, with average values ranging from 41.65 Hz to 41.12 Hz. This confirms that the resonant frequency exhibits negligible temperature sensitivity for the polymer-based cantilever structure.

Fig. 6(b) shows the temperature-dependent RMS voltage output. The experimental average voltage increases from 8.58 V at -20 °C to 13.36 V at 50 °C, with a value of 12.39 V near room temperature (25 °C). The simulated results follow a similar trend, increasing from 9.91 V to 14.32 V over the same range. This increase is nonlinear in nature, especially evident in the 0–40 °C interval, where the slope of the curve gradually flattens. Therefore, instead of assigning a constant rate of increase, we describe the voltage-temperature relationship as a smooth, saturating function. This curvature reflects the inherent material response of the polymer and temperature-dependent changes in the piezoelectric coupling and internal impedance. Notably, voltage output is lower at sub-zero temperatures and rises more rapidly between 0 °C and 30 °C than beyond 30 °C.

Power output, shown in Fig. 6(c), mirrors the voltage behavior. The experimental average power rises from 246.39 µW at -20 °C to 596.40 µW at 50 °C, reaching approximately 500 µW around room temperature. The simulation shows slightly higher outputs, ranging from 329.00 µW to 710.14 µW across the temperature span. The increasing but nonlinear trend suggests improving energy harvesting efficiency with temperature, likely due to enhanced mechanical-to-electrical conversion and reduced energy losses. As with voltage, the curvature in the power response implies that polynomial or exponential fitting may be more appropriate than linear assumptions for model calibration or performance predictions. However, there seems to be a lower voltage generation in the negative temperature region. Interestingly, the rate at which the voltage generation decreases below 0 °C is higher than the rate at which the voltage generation increases after room temperature.

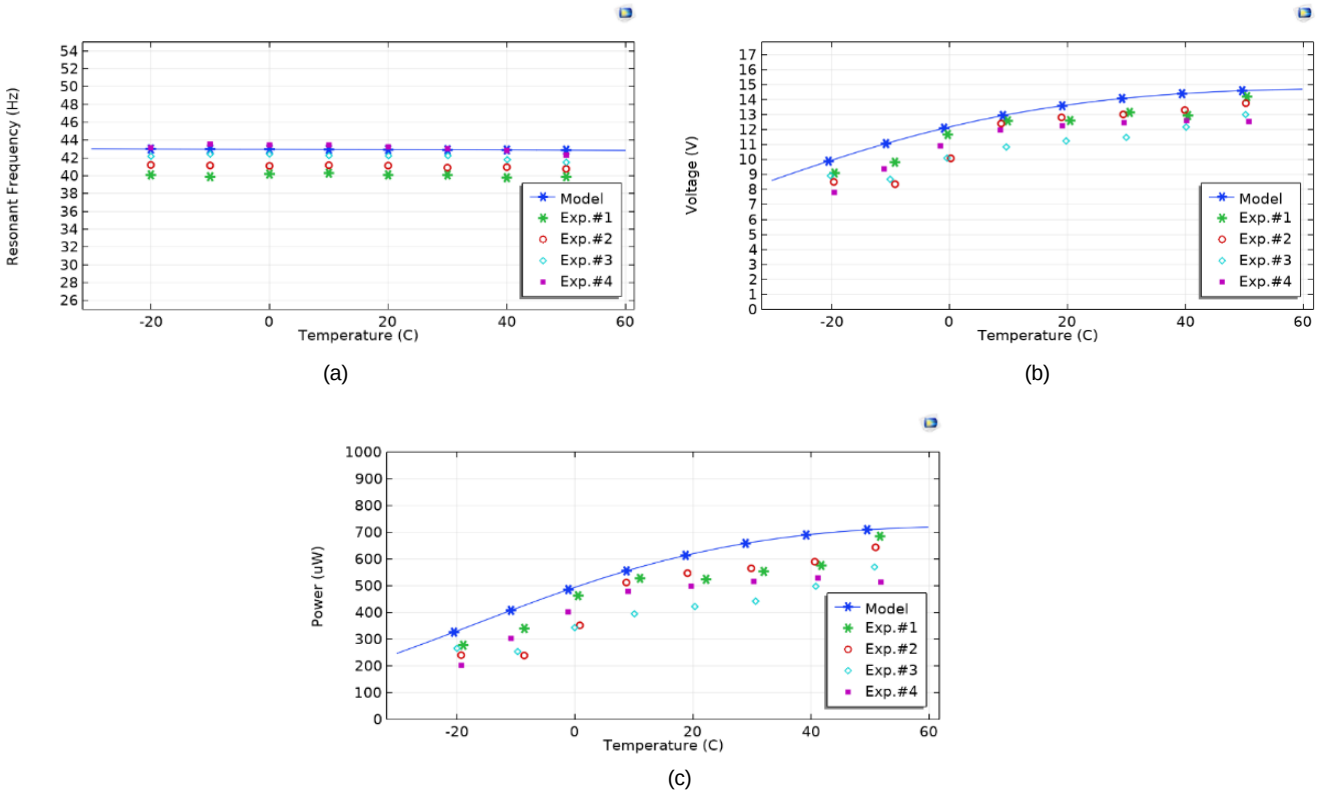

Fig. 6. (a) Resonant frequency verses Temperature change; (b) RMS voltage verses Temperature change; (c) Power generated vs Temperature change.

VIII. Statistical Evaluation

It was evaluated the output voltage and power of four energy harvester devices across a broad range of ambient temperatures (from –20 °C to 50 °C in 10 °C increments). For each temperature setpoint, the open-circuit output of four nominally identical harvesters (devices #1-#4) was measured, and key statistical metrics were computed: mean, standard error (SE), median, standard deviation (SD), variance, range (absolute and percentage), minimum (min), maximum (max), and the 95% confidence interval (CI). These metrics, summarized in Table 4 (voltage) and Table 5 (power), allow us to compare the performance of the harvesters among each other and to assess how temperature influences both the central tendency and variability of their outputs.

This article has been accepted for publication in IEEE Sensors Journal. This is the author's version which has not been fully edited and content may change prior to final publication. Citation information: DOI 10.1109/JSEN.2025.3622932

TABLE IV
STATISTICAL ANALYSIS OF VOLTAGE VS TEMPERATURE

Temp (ºC)	−20				−10				0				10				20				30				40				50			
Harvester No.	1	2	3	4	1	2	3	4	1	2	3	4	1	2	3	4	1	2	3	4	1	2	3	4	1	2	3	4	1	2	3	4
Voltage (V)	9.07	8.52	8.93	7.82	9.55	8.23	8.68	9.87	11.69	10.01	10.15	11.17	12.58	12.70	10.88	12.05	12.62	12.84	11.23	12.22	13.24	13.02	11.47	12.44	12.86	13.30	12.16	12.60	14.15	13.71	12.97	12.64
Mean (V)	8.58				9.08				10.76				12.05				12.23				12.55				12.73				13.36			
Std Err	0.28				0.38				0.40				0.42				0.36				0.40				0.24				0.34			
Median (V)	8.73				9.12				10.66				12.31				12.42				12.73				12.73				13.34			
Std Dev (V)	0.56				0.76				0.81				0.83				0.71				0.79				0.48				0.69			
Var (V*V)	0.32				0.57				0.65				0.69				0.51				0.63				0.23				0.47			
Range %	14.57				18.00				15.62				15.10				13.14				14.12				8.99				11.28			
Range (V)	1.25				1.63				1.68				1.82				1.61				1.77				1.14				1.51			
Min (V)	7.82				8.23				10.01				10.88				11.23				11.47				12.16				12.64			
Max (V)	9.07				9.87				11.69				12.70				12.84				13.24				13.30				14.15			
CI (95%)	0.89				1.21				1.29				1.32				1.13				1.26				0.76				1.09			

TABLE V
STATISTICAL ANALYSIS OF POWER GENERATED VS TEMPERATURE

Temp (ºC)	−20				−10				0				10				20				30				40				50			
Harvester No.	1	2	3	4	1	2	3	4	1	2	3	4	1	2	3	4	1	2	3	4	1	2	3	4	1	2	3	4	1	2	3	4
Power (uW)	274	242	266	204	304	226	251	324.4	455.6	334.1	343.5	415.4	527.7	537.4	394.4	483.5	530.5	549.1	420.3	497.7	584.5	565.3	438.6	515.8	551	589.4	492.3	528.6	666.9	626	560.4	532
Mean (V)	246.39				276.30				387.17				485.74				499.42				526.06				540.35				596.40			
Std Err	15.78				22.86				29.16				32.63				28.42				32.53				20.33				30.61			
Median (V)	253.87				277.51				379.47				505.60				514.10				540.53				539.84				593.21			
Std Dev (V)	31.56				45.71				58.32				65.25				56.85				65.07				40.66				61.21			
Var (V*V)	996.18				2089.68				3401.08				4257.84				3231.62				4233.68				1653.35				3746.70			
Range %	28.57				35.68				31.38				29.43				25.79				27.73				17.96				22.55			
Range (V)	70.39				98.58				121.50				142.95				128.81				145.87				97.04				134.51			
Min (V)	203.72				225.79				334.13				394.40				420.34				438.65				492.35				532.34			
Max (V)	274.11				324.37				455.63				537.35				549.15				584.52				589.39				666.85			
CI (95%)	50.22				72.74				92.80				103.83				90.46				103.54				64.70				97.40			

A. Voltage Output vs Temperature

Mean and Median Voltage. The mean output voltage across the four harvesters increases markedly with ambient temperature. At the lowest temperature of -20 °C, the average voltage is 8.585 V, and this climbs steadily to 13.365 V at 50 °C (Table 2). This ~56 % increase in mean voltage from -20 °C to 50 °C indicates a strong positive correlation between temperature and the generated voltage. The median voltage at each temperature closely tracks the mean (differing by less than ~2 % in all cases), which suggests the voltage values of the four devices are fairly symmetrically distributed without severe outliers. For instance, at 20 °C the mean voltage is 12.226 V and the median is 12.419 V, and at 40 °C both the mean and median coincide at 12.727 V (Table 4). This near coincidence of mean and median shows that no single harvester is dramatically skewing the distribution – the devices' performances are relatively consistent with each other in terms of central tendency.

Variation Among Harvesters. Although the four harvesters show similar overall trends, there are measurable variations in output at each temperature. The standard deviation (SD) of the voltages provides a quantitative measure of this device-to-device variability. At –20 °C, SD ≈ 0.562 V, which corresponds to a coefficient of variation (CV = SD/mean) of about 6.5%. The variation among devices initially increases as temperature

rises to –10 °C (SD ≈ 0.757 V) and 0 °C (SD ≈ 0.808 V). The largest absolute spread in voltage is observed around 10 °C, where SD = 0.832 V and the range spans 1.819 V (from 10.879 V up to 12.698 V). In relative terms, at -10 °C the range is about 1.635 V, which is ~18% of the 9.08 V mean – this is the highest percentage variation seen in the voltage data. Beyond 10 °C, the device outputs begin to converge slightly: by 30–40 °C the variation is lower (SD ~0.69 V at 30 °C, dropping to 0.479 V at 40 °C). Overall, the relative variation (range%) among devices stays within 9–18% across the entire temperature sweep for voltage. Such levels of device scatter are in line with what has been observed in other studies of fabricated energy harvesters – for example, Xu et al.[32] reported around 30% relative standard deviation in peak output voltage across a batch of 40 MEMS piezoelectric harvesters. Our four devices show a smaller spread (SD is at most ~8% of the mean, and typically ~4–7% at moderate temperatures), indicating a reasonably good uniformity for a small sample. Nonetheless, the presence of any variation highlights the influence of fabrication differences or material inconsistencies on performance. These device-specific differences are consistent with minor parameter variations; importantly, their effect diminishes at the intermediate temperature of 40 °C where all devices converge tightly.

Standard Error and Confidence Interval. The standard error (SE) of the mean voltage, given by SD/√n (with n=4 devices), reflects the uncertainty in the estimated mean at each temperature. At most temperatures the SE is a few tenths of a volt (e.g. 0.416 V at 10 °C), and it reaches a minimum of 0.240 V at 40 °C thanks to the low scatter there. The corresponding 95% confidence interval (CI) for the mean can be calculated (for n=4, using the t-distribution) – this interval width is about ±(3.18·SE). For example, at 10 °C the mean voltage 12.05 V has a 95% CI of approximately ±1.324 V, i.e. one can be 95% confident the true mean lies between ~10.73 V and ~13.38 V given the device-to-device variability. At 40 °C, the CI narrows to about ±0.763 V around the 12.727 V mean. In general, the 95% CI spans were on the order of 0.8–1.3 V (Table 4) – relatively small compared to the mean values – indicating that despite the limited sample of 4 devices, the mean output at each temperature is estimated with decent precision.

It is worth noting that the largest relative disparities occurred in the sub-zero region. At –10 °C, one harvester (Device #2) lagged significantly (8.23 V versus ~9.55 V for the best device), contributing to the highest variance and range%. This could be related to performance issues at low temperatures, such as increased internal impedance or even environmental effects like frost/condensation. Indeed, previous work has observed anomalies in harvester output around freezing conditions – Xu et al. reported a “clear break” in device behavior at 0 °C, likely due to condensation forming on the device. Our results align with that observation: between –10 °C and 0 °C the average voltage jumped from 9.08 V to 10.76 V (a larger step than in other intervals), and the device which was weakest at –10 °C recovered by 0 °C, suggesting that transient effects (possibly moisture-related) impacted the –10 °C readings. Above 0 °C, the devices’ outputs increase smoothly, and the variation trends become more stable. Overall, the statistical analysis of voltage outputs confirms that higher temperatures significantly boost the harvested voltage, while also slightly improving the uniformity among devices at certain mid-high temperatures.

B. Power Output vs Temperature

Output power vs ambient temperature for four harvesters. Each device’s power output (in μW) is plotted as a function of temperature. Power increases steeply with temperature for all harvesters, roughly doubling (or more) between the lowest and highest temperatures. The spread in power outputs between devices is more pronounced at lower temperatures (e.g. at –10 °C) and narrows at certain higher temperatures (e.g. 40 °C), reflecting the amplified effect of voltage variation on power.

In summary, the power analysis confirms that higher temperatures substantially boost the energy harvesting capability, more than doubling the average power from –20 °C to 50 °C. Concurrently, the relative differences between devices become less extreme at higher temperatures (with the exception of the very highest point where one device excelled). The data suggest that around 30–40 °C, the harvesters not only output high power (~0.5–0.55 mW on average) but also operate uniformly, which could be an ideal operating window for reliable deployment of such devices. The insights gained from these statistical metrics – mean trends and variability measures – are valuable for both the design and application of energy harvesters. They illustrate how environmental temperature can affect not just the expected power output but also the performance spread among units, which is crucial for predicting system behavior and for quality control of the harvesters. Future work may compare these results with other studies or theoretical models; for instance, our observed temperature coefficient of voltage is consistent with the fundamental thermoelectric effect, and the device-to-device variation we quantified (~10–30% range in power) is in line with prior experimental reports for small batches of harvesters.

IX. DISCUSSION AND COMPARISON WITH EXISITNG WORKS

Quantitatively, the deviations between experimental medians and simulated values are generally small: on the order of 1% for frequency, 5–15% for voltage, and 5–12% for power. Most of these differences fall within or just above the predefined tolerance ranges for each metric (with only the low-temperature voltage deviation significantly exceeding the ±5% voltage criterion). The fact that simulation and experiment converge at the high-temperature end for all outputs boost confidence that the model captures the essential physics and that any disparities at low temperature could be addressed by refining material property inputs (e.g. temperature-dependent modulus or damping in the simulation [33], [34].).

At lower temperatures, the material became harder, and its stiffness increased. A rigid cantilever means smaller amplitudes of vibrations hence smaller output RMS voltage and power generation is observed at lower temperatures. because the mechanical stiffness of the base steel increases. However, at higher temperatures, with a softer core, the same acceleration produces more voltage.

At lower temperatures, the steel substrate exhibits increased stiffness due to reduced atomic vibrations, leading to higher Young's modulus values [35]. This increased stiffness results in

diminished vibrational amplitudes under the same excitation, thereby reducing the mechanical strain transferred to the piezoelectric layer and consequently lowering the output RMS voltage and power generation. Conversely, as the temperature rises, the steel becomes more compliant, allowing for greater vibrational amplitudes and enhances energy conversion efficiency.

The piezoelectric polymer layer, such as PVDF, also exhibits temperature-dependent behavior. As temperature increases, the piezoelectric coefficients (e.g., d_31) can initially increase due to enhanced molecular mobility [36], improving the material's ability to convert mechanical energy into electrical energy. However, beyond a certain temperature threshold, these coefficients may decrease due to depolarization effects [37].

Equally important, the consistency of the four harvesters' performance is evident from the tight clustering of the box plots at each temperature. The devices demonstrate uniform behavior, confirming that the observed trends are intrinsic to the harvester design rather than random unit-to-unit variations. This consistency, even when pushed to –20°C and 50°C, speaks to the reliability of both the materials and the fabrication process. Only slight increases in output scatter at the extremes hint at the expected challenges (for instance, polymers stiffening in the cold or reaching softening points when hot), but these effects are relatively minor. All harvesters remained operational and effective throughout, with no outliers falling outside the whisker ranges to indicate any device failure or aberrant performance.

The resonant frequency is practically invariant with temperature, ensuring consistent device tuning, while the voltage and power outputs improve with temperature in line with theoretical expectations (higher piezoelectric activity and lower internal losses at warmer temperatures). The deviations between experiment and simulation are quantitatively small and mostly within acceptable engineering tolerances, highlighting the model's validity. Furthermore, the small variability among devices confirms a high level of reproducibility and reliability in the harvester design.

This proposed EH device within a volume of 270 mm^3 shows an output power of up to 1mW which is comparable to that of the best-performing PVDF-based energy harvesters within similar volume reported so far [38], [39]. For comparison, these features of the energy harvester are tabulated along with other published works in Table VI. The RMS voltage generated by EH is more than 5 times that of the piezo sensors that are available commercially. The proposed harvester power density is nearly ten thousand times more than that of commercial piezo sensors, shown in our previous works [40] .

Our device achieves a power density of 3.77 μW/g/mm³ at room temperature, which is competitive with current state-of-the-art piezoelectric energy harvesters. For instance, recent studies have reported power densities ranging from 0.035 3.77 μW/g/mm³ to 1.22 μW/g/mm³ under various conditions and materials. While direct comparisons are challenging due to differences in materials, device architectures, and testing conditions, our results demonstrate that our device performs favorably within the context of existing technologies.

The power output of the proposed energy harvester exhibits a clear temperature-dependent behavior, with experimental results showing a nonlinear increase in power as temperature rises from −20 °C to 50 °C under constant excitation. Although a precise power density of 3.77 μW/g/mm³ is achieved at room temperature, performance at lower temperatures is reduced due to increased material stiffness, which limits cantilever deflection and energy conversion efficiency. Conversely, higher temperatures enhance flexibility and improve output. These trends align well with theoretical expectations of temperature-dependent material properties—particularly in polymers like PVDF, where piezoelectric coupling improves with thermal softening up to a certain threshold. Compared to recent state-of-the-art PVEH systems using rigid piezoceramics, our polymer-based device offers competitive performance while providing advantages in flexibility and durability. This positions the proposed design as a promising candidate for practical applications where moderate temperature fluctuations are expected, especially in wearable, structural, and automotive environments.

TABLE VI
SUMMARY OF RELATED WORKS

Sl No	f_{res} (Hz)	$P_{Density}\left(\frac{\mu W/mm^3}{g}\right)$	Ref
1	33	0.035	[41]
2	30	0.116	[42]
3	17	0.15	[43]
4	30.8	0.220	[44]
5	55	0.38	[45]
6	103.8	0.94	[46]
7	34.4	1.22	[47]
8	43	3.77	Our Proposal

X. CONCLUSION

Our experimental data demonstrates a clear, nonlinear increase in power output with temperature. Specifically, the average power output rises from 246.39 μW at −20 °C to 596.40 μW at 50 °C, with a notable acceleration in growth between 0 °C and 30 °C. This trend is mirrored in our simulations, which show power increasing from 329.00 μW to 710.14 μW over the same temperature range.

The observed temperature-dependent behavior aligns with established theoretical models of piezoelectric materials. As temperature increases, the mechanical stiffness of the steel substrate decreases, allowing for greater vibrational amplitudes and enhanced strain transfer to the piezoelectric layer. Concurrently, the piezoelectric polymer (e.g., PVDF) exhibits increased molecular mobility, leading to enhanced piezoelectric coefficients up to a certain temperature threshold. These combined effects result in increased voltage and power output at elevated temperatures. Similar temperature-dependent enhancements in piezoelectric performance have been reported in the literature, corroborating our findings.

Rayleigh damping coefficients ($\alpha_1 = 0.51$, $\alpha_2 = 1.04\times10^{-6}$) were experimentally extracted and applied in COMSOL to accurately simulate energy harvester (EH) performance. Their inclusion significantly improved alignment between simulated and measured power outputs across temperature ranges.

PVDF was validated as a viable piezoelectric material for EH applications within 0 °C to 60 °C. Results provide practical guidance on operational limits, safe temperature thresholds, and

long-term reliability of EH devices. The developed harvester demonstrated a power density of 3.77 μW/g/mm³, placing it on par with conventional PZT-based harvesters despite using flexible polymeric materials.

Quantitatively, the deviations between experimental medians and simulated values are generally small: on the order of 1% for frequency, 5–15% for voltage, and 5–12% for power. Most of these differences fall within or just above the predefined tolerance ranges for each metric (with only the low-temperature voltage deviation significantly exceeding the ±5% voltage criterion). Such a strong correlation between experimental data and simulation not only validates the design and modeling approach but also provides confidence for deploying these harvesters in real-world environments with fluctuating temperatures.

To the authors' knowledge, this is the first integrated experimental and simulation study analyzing temperature effects on a full PVDF-based EH system. The methodology offers a foundation for future studies on thermal aging, service life prediction, and optimization of polymer-based harvesters.

The authors plan to investigate the performance of piezoelectric energy harvesters using flexible polymer substrates, such as polypropylene (PP) and polyethylene terephthalate (PET), to assess their thermal and mechanical behavior across varying temperatures. The current study establishes foundational measurements, while the investigation of accelerated thermal aging, long-term durability, and performance optimization will be addressed in a separate follow-up study. This future research aims to explore the potential advantages of polymer substrates over traditional steel, including enhanced flexibility and reduced weight, which could lead to improved energy harvesting efficiency in diverse applications.

XI. ACKNOWLEDGMENT

This research has received funding from the Research Council of Lithuania (LMTLT), agreement No S-A-UEI-23-1 (22-12-2023).

REFERENCES

[1] J. Hund, H. M. Granum, S. N. Olufsen, P. H. Holmström, J. Johnsen, and A. H. Clausen, "Impact of stress triaxiality, strain rate, and temperature on the mechanical response and morphology of PVDF," *Polym Test*, vol. 114, p. 107717, Oct. 2022, doi: 10.1016/J.POLYMERTESTING.2022.107717.

[2] P. H. Jain and S. P. Bhosle, "Mathematical modeling, simulation and analysis of non-linear vibrations of a ball bearing due to radial clearance and number of balls," *Mater Today Proc*, vol. 72, pp. 927–936, 2023, doi: 10.1016/J.MATPR.2022.09.093.

[3] "Properties and Uses of Polyvinylidene Fluoride - Alfa Chemistry." Accessed: May 07, 2025. [Online]. Available: https://www.alfa-chemistry.com/resources/properties-and-uses-of-polyvinylidene-fluoride.html

[4] T. Kelley, "Effect of temperature on the pulse-echo performance of ultrasonic transducers fabricated with PVDF film," *IET Science, Measurement and Technology*, vol. 13, no. 3, 2019, doi: 10.1049/iet-smt.2018.5453.

[5] M. Cepenas *et al.*, "Research of parameters of plastic piezoelectric harvester for practical model implementation," *13th International Conference ELEKTRO 2020, ELEKTRO 2020 - Proceedings*, vol. 2020-May, 2020, doi: 10.1109/ELEKTRO49696.2020.9130273.

[6] D. Garcia-Gonzalez, S. Garzon-Hernandez, A. Rusinek, R. Bernier, and A. Arias, "Low temperature mechanical behaviour of PVDF: cryogenic pre-treatment, quasi-static, cyclic and dynamic experimental testing and modelling," *Mechanics of Materials*, vol. 147, no. April, p. 103436, Aug. 2020, doi: 10.1016/j.mechmat.2020.103436.

[7] M. Cepenas *et al.*, "Research of pvdf energy harvester cantilever parameters for experimental model realization," *Electronics (Switzerland)*, vol. 9, no. 12, pp. 1–14, 2020, doi: 10.3390/electronics9122030.

[8] S. Ray and R. P. Cooney, "Thermal degradation of polymer and polymer composites," *Handbook of Environmental Degradation Of Materials: Third Edition*, pp. 185–206, Jun. 2018, doi: 10.1016/B978-0-323-52472-8.00009-5.

[9] S. Ray, A. K. Bhowmick, and S. Swayajith, "Influence of untreated and novel electron-beam-modified surface-coated silica filler on the thermorheological properties of ethylene-octene copolymer," 2003. doi: 10.1002/app.12938.

[10] A. K. Bhowmick, S. Ray, A. M. Shanmugharaj, J. Heslop, N. Köppen, and J. R. White, "Photomechanical degradation of thermoplastic elastomers," *J Appl Polym Sci*, vol. 99, no. 1, pp. 150–161, Jan. 2006, doi: 10.1002/APP.21913.

[11] J. D. Peterson, S. Vyazovkin, and C. A. Wight, "Kinetics of the thermal and thermo-oxidative degradation of polystyrene, polyethylene and poly(propylene)," *Macromol Chem Phys*, vol. 202, no. 6, pp. 775–784, 2001, doi: 10.1002/1521-3935(20010301)202:6<775::AID-MACP775>3.0.CO;2-G.

[12] C. R. Siviour, S. M. Walley, W. G. Proud, and J. E. Field, "The high strain rate compressive behaviour of polycarbonate and polyvinylidene difluoride," *Polymer (Guildf)*, vol. 46, no. 26, pp. 12546–12555, Dec. 2005, doi: 10.1016/j.polymer.2005.10.109.

[13] Y. P. Neo *et al.*, "Influence of Heat Curing on Structure and Physicochemical Properties of Phenolic Acid Loaded Proteinaceous Electrospun Fibers," *J Agric Food Chem*, vol. 62, no. 22, pp. 5163–5172, Jun. 2014, doi: 10.1021/JF500841M.

[14] M. C. Celina, "Review of polymer oxidation and its relationship with materials performance and lifetime prediction," *Polym Degrad Stab*, vol. 98, no. 12, pp. 2419–2429, Dec. 2013, doi: 10.1016/J.POLYMDEGRADSTAB.2013.06.024.

[15] E. P. Motta, J. M. L. Reis, and H. S. da Costa Mattos, "Analysis of the cyclic tensile behaviour of an elasto-viscoplastic polyvinylidene fluoride (PVDF)," *Polym Test*, vol. 67, pp. 503–512, May 2018.

[16] A. Santimetaneedol, R. Tripuraneni, S. A. Chester, and S. P. V. Nadimpalli, "Time-dependent deformation behavior of polyvinylidene fluoride binder: Implications on the mechanics of composite electrodes," *J Power Sources*, vol. 332, pp. 118–128, Nov. 2016, doi: 10.1016/j.jpowsour.2016.09.102.

[17] I. Izadgoshasb, Y. Y. Lim, N. Lake, L. Tang, R. V. Padilla, and T. Kashiwao, "Optimizing orientation of piezoelectric cantilever beam for harvesting energy from human walking," *Energy Convers Manag*, vol. 161, pp. 66–73, Apr. 2018, doi: 10.1016/J.ENCONMAN.2018.01.076.

[18] N. H. H. Mohamad Hanif, A. Jazlan Mohaideen, H. Azam, and M. E. Rohaimi, "Rotational piezoelectric energy harvester for wearable devices," *Cogent Eng*, vol. 5, no. 1, p. 1430497, Jan. 2018, doi: 10.1080/23311916.2018.1430497/ASSET/FFD2B4C4-BECF-4D6E-ADBA-33721474F4D3/ASSETS/IMAGES/LARGE/OAEN_A_1430497_F0008_B.JPG.

[19] C. P. Okeke, A. N. Thite, J. F. Durodola, N. A. Fellows, and M. T. Greenrod, "Modelling of hyperelastic polymers for automotive lamps under random vibration loading with proportional damping for robust

fatigue analysis," *Procedia Structural Integrity*, vol. 13, pp. 1460–1469, 2018, doi: 10.1016/J.PROSTR.2018.12.302.

[20] P. Jehel and R. Cottereau, "On damping created by heterogeneous yielding in the numerical analysis of nonlinear reinforced concrete frame elements," *Comput Struct*, vol. 154, pp. 192–203, Jul. 2015, doi: 10.1016/j.compstruc.2015.03.001.

[21] X. Lu *et al.*, "Design and Testing of Cantilevered PVDF Energy Harvester Based on the Coanda Effect," *IEEE Access*, vol. 8, pp. 19606–19613, 2020, doi: 10.1109/ACCESS.2020.2968218.

[22] J. W. Yi, W. Y. Shih, and W. H. Shih, "Effect of length, width, and mode on the mass detection sensitivity of piezoelectric unimorph cantilevers," *J Appl Phys*, vol. 91, no. 3, pp. 1680–1686, 2002, doi: 10.1063/1.1427403.

[23] T. Furukawa, "Piezoelectricity and Pyroelectricity in Polymers," *IEEE Transactions on Electrical Insulation*, vol. 24, no. 3, pp. 375–394, 1989, doi: 10.1109/14.30878.

[24] "Computing Rayleigh Damping Coefficients | Knowledge Base | SimScale." Accessed: May 06, 2025. [Online]. Available: https://www.simscale.com/knowledge-base/rayleigh-damping-coefficients/

[25] G. Tehrani, ˙ Ilker Bülbül, M. Akda, and H. Karagülle, "Active Vibration Control of Cantilever Structures by Integrating the Closed Loop Control Action into Transient Solution of Finite Element Model and an Application to Aircraft Wing," *Machines 2025, Vol. 13, Page 379*, vol. 13, no. 5, p. 379, Apr. 2025, doi: 10.3390/MACHINES13050379.

[26] D. Mažeika, A. Čeponis, and Y. Yang, "Multifrequency Piezoelectric Energy Harvester Based on Polygon-Shaped Cantilever Array," *Shock and Vibration*, vol. 2018, 2018, doi: 10.1155/2018/5037187.

[27] "Estimating Damping with Logarithmic Decrement in DSDOF Systems." Accessed: May 06, 2025. [Online]. Available: https://www.structuralengineeringsimplified.com/dynamics/dsdof/logdecrement?utm_source=chatgpt.com

[28] A. I. Yusuf and N. M. Amin, "Determination of Rayleigh Damping Coefficient for Natural Damping Rubber Plate Using Finite Element Modal Analysis", doi: 10.1007/978-981-287-290-6_62.

[29] P. Subudhi, V. Sagar, S. Kumar, and D. Punetha, "Simulation and Optimization of Substrate Layer Material for PVDF Cantilever Based Vibration Energy Harvesting System," *IEEE Sens J*, vol. 23, no. 23, pp. 28689–28695, Dec. 2023, doi: 10.1109/JSEN.2023.3326681.

[30] S. Baishya, D. Borthakur, R. Kashyap, and A. Chatterjee, "A High Precision Lumped Parameter Model for Piezoelectric Energy Harvesters," *IEEE Sens J*, vol. 17, no. 24, pp. 8350–8355, Dec. 2017, doi: 10.1109/JSEN.2017.2764165.

[31] C. A. Bernard, J. P. M. Correia, S. Ahzi, and N. Bahlouli, "Numerical implementation of an elastic-viscoplastic constitutive model to simulate the mechanical behaviour of amorphous polymers," *International Journal of Material Forming*, vol. 10, no. 4, pp. 607–621, Aug. 2017, doi: 10.1007/s12289-016-1305-8.

[32] R. Xu *et al.*, "Preliminary performance evaluation of MEMS-based piezoelectric energy harvesters in extended temperature range," in *Procedia Engineering*, Elsevier Ltd, 2012, pp. 1434–1437. doi: 10.1016/j.proeng.2012.09.427.

[33] E. Finot, A. Passian, and T. Thundat, "Measurement of mechanical properties of cantilever shaped materials," *Sensors*, vol. 8, no. 5, 2008, doi: 10.3390/s8053497.

[34] J. Han, C. Zhu, J. Liu, and Y. He, "Dependence of the resonance frequency of thermally excited microcantilever resonators on temperature," *Sens Actuators A Phys*, vol. 101, no. 1–2, 2002, doi: 10.1016/S0924-4247(02)00146-2.

[35] S. By and B. A. Hall, "PIEZOELECTRIC ENERGY HARVESTING UTILIZING METALLIZED POLY-VINYLIDENE FLUORIDE (PVDF)."

[36] H. Elahi, M. Eugeni, and P. Gaudenzi, "A review on mechanisms for piezoelectric-based energy harvesters," 2018, *MDPI AG*. doi: 10.3390/en11071850.

[37] A. Garg, S. Agarwal, and D. Punetha, "Polarization and Strain in Piezoelectric Nanomaterials: Advancing Sensing Applications in Biomedical Technology," *IEEE Open Journal of Nanotechnology*, 2024, doi: 10.1109/OJNANO.2024.3488787.

[38] S. C. Mukhopadhyay, "Wearable sensors for human activity monitoring: A review," *IEEE Sens J*, vol. 15, no. 3, pp. 1321–1330, 2015, doi: 10.1109/JSEN.2014.2370945.

[39] M. Jamshed, K. Ali, Q. Abbasi 2022, "Challenges, applications, and future of wireless sensors in Internet of Things: A review," *ieeexplore.ieee.org*, Accessed: Aug. 21, 2024. [Online]. Available: https://ieeexplore.ieee.org/abstract/document/9698203/?casa_token=PmWpar7sEuAAAAAA:ghCbvHF1OQnxvJK9wcMNfmejxodiER-g0OdWrvGfw31IoO4Q3UljjwqCorAUWoFS9xu0fF8QMQ

[40] C. Ravikumar, V. Markevicius, D. Navikas, B. Peng, and D. Andriukaitis, "Comparison of Performance of PVDF-based Piezoelectric Energy Harvester with Commercial Piezo Sensor," in *Proceedings of the 2022 26th International Conference Electronics, ELECTRONICS 2022*, Institute of Electrical and Electronics Engineers Inc., 2022. doi: 10.1109/IEEECONF55059.2022.9810393.

[41] S. Rammohan, S. Chiplunkar, C. M. Ramya, S. J. Kumar, and A. Jain, "Multi-layer Piezoelectric Energy Harvesters for Improved Power Generation," no. Figure 1, pp. 1–6, 2014.

[42] S. Rammohan, C. Ramya, S. Jayanth Kumar, J. Anjana, and P. Rudra, "Low frequency vibration energy harvesting using arrays of PVDF piezoelectric bimorphs," *Journal of institute of smart structures ans systems*, vol. 3, no. 1, pp. 18–27, 2014.

[43] Y. Jiang, S. Shiono, H. Hamada, T. Fujita, K. Higuchi, and K. Maenaka, "LOW-FREQUENCY ENERGY HARVESTING USING A LAMINATED PVDF CANTILEVER WITH A MAGNETIC MASS Maenaka Human-Sensing Fusion Project , Japan Science and Technology Agency , Himeji , Japan," no. November, 2009.

[44] R. Sriramdas, S. Chiplunkar, R. M. Cuduvally, and R. Pratap, "Performance enhancement of piezoelectric energy harvesters using multilayer and multistep beam configurations," *IEEE Sens J*, vol. 15, no. 6, pp. 3338–3348, 2015, doi: 10.1109/JSEN.2014.2387882.

[45] H. Takise, T. Takahashi, M. Suzuki, and S. Aoyagi, "Fabrication of piezoelectric vibration energy harvester using coatable PolyVinylidene DiFluoride and its characterisation," *Micro Nano Lett*, vol. 12, no. 8, pp. 569–574, 2017, doi: 10.1049/mnl.2017.0128.

[46] Z. Cao, J. Zhang, and H. Kuwano, "Vibration energy harvesting characterization of 1 cm2 poly(vinylidene fluoride) generators in vacuum," *Jpn J Appl Phys*, vol. 50, no. 9 PART 3, pp. 13–17, 2011, doi: 10.1143/JJAP.50.09ND15.

[47] J. Song, G. Zhao, B. Li, and J. Wang, "Design optimization of PVDF-based piezoelectric energy harvesters," *Heliyon*, vol. 3, no. 9, p. e00377, Sep. 2017, doi: 10.1016/J.HELIYON.2017.E00377.

Chandana Ravikumar received a degree in Bachelor of Electrical and Electronics Engineering, from Visvesvaraya Technological University, Bengaluru, India in 2018. and MSc degree and PhD from the Electronics Department, Kaunas University of Technology, Lithuania in 2020 and 2024. She did her first post-doctoral research at CTU- University Centre for Energy Efficient Buildings, department for monitoring and intelligent control of buildings (Czech Republic). She currently works as a Marie Sklodowska-Curie Postdoctoral Fellow (MSCA-PF) CZ OPJAK at the Faculty of Mathematics and Physics in Charles University Prague. Her research interests include digital signal processing, low-power smart sensors,

timber construction monitoring systems and structural health monitoring, MEMS, Battery management systems, metallurgy and finite element analysis.
https://orcid.org/0000-0002-2788-0170

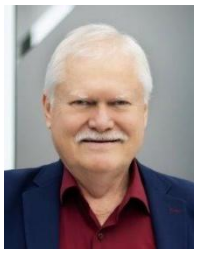

Vytautas Markevičius graduated MSc in 1973 and received Ph.D. in Electronics Engineering in 1983. He works at the Department of Electronics Engineering, Faculty of Electrical and Electronics Engineering, Kaunas University of Technology. The leader of the research group on Interactive electronic systems. His research focuses on finding solutions for the issues related to interactive electronic systems, integrated information systems, energy harvesting, low power management, and WSN.
https://orcid.org/0000-0001-8856-1037

Dangirutis Navikas graduated MSc in 1994 and received Ph.D. in Electronics Engineering in 1999. He works at the Department of Electronics Engineering, Faculty of Electrical and Electronics Engineering, Kaunas University of Technology. Also, he is the head of the Department of Electronics Engineering. His research focuses on finding solutions for the issues related to the interactive design of microprocessor systems, integrated information systems, or WSN.
https://orcid.org/0000-0001-7071-7566

Mindaugas Čepėnas graduated from Kaunas University of Technology (KTU) in 2012 with a Master's degree in Electronics Engineering. He was awarded his Ph.D. in 2018 in the field of Electronics Engineering. He works as a researcher at the Department of Electronics Engineering, Faculty of Electrical and Electronics Engineering, Kaunas University of Technology. His research focuses on electronic system efficiency, energy harvesting, low power management, and wireless smart sensors.
https://orcid.org/0000-0002-0887-0161

Algimantas Valinevičius graduated MSc in 1979 and received PhD in Electronics Engineering in 1986. He works at Department of Electronics Engineering, Faculty of Electrical and Electronics Engineering, Kaunas University of Technology. Also, he is a dean of the Faculty of Electrical and Electronics Engineering. His research focuses on finding solutions for the issues related to interactive electronic systems, integrated information systems or WSN.
https://orcid.org/0000-0002-8604-9678

Mindaugas Žilys graduated MSc in 1996 and received PhD in Electronics Engineering in 2001. He works as a researcher at Department of Electronics Engineering, Faculty of Electrical and Electronics Engineering, Kaunas University of Technology and in industry. His research focuses on electronic system efficiency, energy harvesting, low power management and wireless smart sensors.
https://orcid.org/0000-0002-6589-0599

Roman Šotner (Member, IEEE) was born in Znojmo, Czech Republic, in 1983. He received the M.Sc. and Ph.D. degrees from Brno University of Technology, Brno, Czech Republic, in 2008 and 2012, respectively. He is currently an Associate Professor with the Department of Radio Electronics, Faculty of Electrical Engineering and Communication, Brno University of Technology. His interests include analog circuits (active filters, oscillators, and audio), circuits in the current mode, circuits with direct electronic controlling possibilities especially, and computer simulation
https://orcid.org/0000-0002-2430-1815

Jan Jerabek was born in Bruntal, Czech Republic, in 1982. He received the B.Sc. and M.Sc. degrees and the Ph.D. degree in electrical engineering from Brno University of Technology, Czech Republic, in 2005, 2007, and 2011, respectively. He is currently an Associate Professor with the Department of Telecommunications, Faculty of Electrical Engineering and Communication, Brno University of Technology. His research interests include analogue signal processing, including circuit design, analyses, and measurements.
https://orcid.org/0000-0001-9487-5024)

Zhixiong Li (Senior Member, IEEE) received the Ph.D. degree in transportation engineering from the Wuhan University of Technology, Wuhan, China. He is currently a Scientific Council Member of the discipline of mechanical engineering with the Faculty of Mechanical Engineering, Opole University of Technology, Poland. His research interests include intelligent vehicles and control, loop closure detection, and mechanical system modeling and control. He is also an Associate Editor of Measurement (Elsevier) and a Column Editor of IEEE Intelligent Transportation Systems Magazine.
https://orcid.org/0000-0002-7265-0008

Jan Včelák Jan Včelák, is a senior researcher in CTU- University Centre for Energy Efficient Buildings, department for monitoring and intelligent control of buildings (Czech Republic). His expertise relates to sensor design for special purposes, and complex sensor systems including data processing algorithms. His activities cover also topic of sustainable building construction materials and sensor system for their diagnostics and monitoring covering fibre optic sensors, timber construction monitoring systems and structural health monitoring
https://orcid.org/0000-0002-0647-2987

Darius Andriukaitis Darius Andriukaitis graduated MSc in 2005 and received Ph.D. in Electronics Engineering in 2009. He works at the Department of Electronics Engineering, Faculty of Electrical and Electronics Engineering, Kaunas University of Technology. Also, he is a vice dean for research at the Faculty of Electrical and Electronics Engineering. His research focuses on finding solutions for issues related to interactive electronic systems, integrated information systems, smart transportation systems, control systems, IoT or WSN. https://orcid.org/0000-0002-9862-8917

XII. Appendix A

A. Rayliegh damping measurements

Polymers such as PVDF, P(VDF-HFP), PMMA, and ABS exhibit viscoelastic behavior [23], meaning their damping characteristics are both time- and frequency-dependent. While Rayleigh damping provides a convenient means to include damping in simulations, the α (mass-proportional damping) and β(stiffness-proportional damping) coefficients are not intrinsic material properties and often require calibration [24]. This calibration is typically performed by matching the simulated damping ratios to experimental data over the frequency range of interest.

For macroscale polymer cantilevers, typical values reported in the literature [19] include α values in the range of 10 to 25 s^{-1}, and β values between 5×10^{-6} and 1×10^{-5} s. For instance, Okeke et al.[19] experimentally determined α = 10.5–23.2 s^{-1} and β = 6.7×10^{-6} to 1.2×10^{-5} s for polymers such as PMMA and ABS by fitting random vibration responses. In another study, β = 5.37×10^{-5} s was used to replicate free vibration decay in a cantilever beam [25].

The procedure is described for determining damping ratios in polymer vibration energy harvesters (PVEHs) and is a well-established method [18] in structural dynamics and materials engineering, A typical underdamped vibration response, shown in Fig. A-1, is described by Eq. (A.1), governed by initial displacement $x(0) = d_0$, and velocity $\dot{x}(0) = v_0$. The solution represents a single-mode harmonic oscillator with exponential decay [18].

$$x(t) = e^{-\zeta_i \omega_n t}\left(d_0 cos\, w_d t + \frac{v_0 + \zeta_i w_n d_0}{w_d} sin\, w_d\, t\right) \quad \text{(A.1)}$$

The terms include initial displacement (d_0) and velocity (v_0), natural (ω_n) and damped (w_d) angular frequencies, damping ratio (ζ_i), time-dependent oscillatory components (cos and sin) and exponential decay ($e^{-\zeta_i \omega_n t}$) due to damping. This expression models the decaying oscillation observed experimentally for a single resonant mode, as depicted in Fig. A-1.

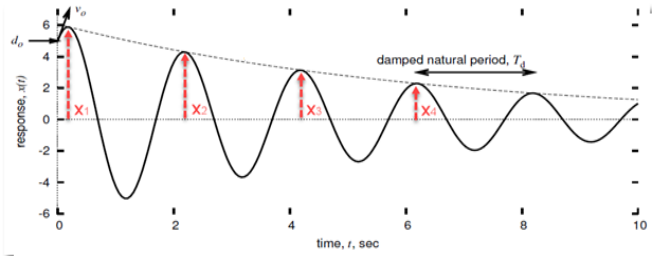

Fig. A-1. Illustration of a typical damped signal.

The goal of the flowchart and experiment setup, seen in Figs. A-1 and A-2 is to determine the damping ratios associated with the PVEH's first and second vibrational modes. This is achieved by measuring the free decay response of the harvester after excitation, using a high-precision laser interferometer setup. The displacement data collected allows for the calculation of the logarithmic decrement, which quantifies the rate at which oscillations diminish over time. Subsequently, these values are used to compute the damping ratios for each mode.

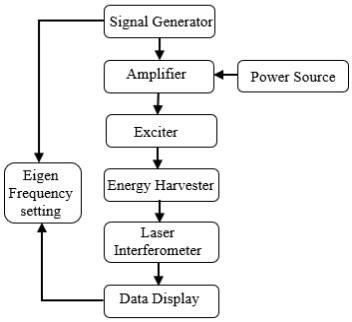

Fig. A-2. Flowchart of the experiment setup.

To initiate oscillation, the energy harvester (EH) was mounted on an exciter system comprising a signal generator, low-frequency amplifier, and power source, as shown in Fig. A-3. For precise displacement measurement of the energy harvester (EH), a dual-frequency helium–neon (He–Ne) laser interferometer was employed, offering extended measurement range without compromising resolution. The interferometer generates two orthogonally polarized beams with a frequency difference of 2×10^6 Hz, derived from a nominal 5×10^{14} Hz source. These beams are split into reference and measurement paths via a beam splitter. The EH, mounted on an exciter driven by a low-frequency amplifier and signal generator, was monitored by positioning the interferometer directly above the cantilever tip. Displacement over time was recorded and visualized on a connected system, as illustrated in Fig. A-4.

The harvester is excited to resonate at its natural frequencies (43 Hz and 163.7 Hz), and upon cessation of excitation, the free decay response is recorded as illustrated in Fig. A-1, A-4. By analyzing the amplitudes of successive peaks in the decay curve, the logarithmic decrement is calculated using the formula [24]:

$$\delta = \frac{1}{n} ln\left[\frac{x(t)}{x(t+nT)}\right] \quad \text{(A.2)}$$

where x(t) and x(t+nT) are the amplitudes of two successive peaks separated by n cycles. The damping ratio ζ is then determined from the logarithmic decrement using [27]:

$$\zeta = \frac{1}{\sqrt{1+\left(\frac{2\pi}{\delta}\right)^2}} \qquad \text{(A.3)}$$

These damping ratios for the two modes are subsequently used to compute the Rayleigh damping coefficients α and β through [28]:

$$\alpha_1 = \frac{2w_1\omega_2}{w_2^2-w_1^2}(\zeta_1\omega_2 - \zeta_2\omega_1) \qquad \text{(A.4)}$$

$$\alpha_2 = \frac{2}{w_2^2-w_1^2}(\zeta_2\omega_2 - \zeta_1\omega_1) \qquad \text{(A.5)}$$

where $\omega_1$and ω_2 are the natural angular frequencies of the first and second modes, respectively. The Rayleigh damping coefficients—mass proportional $0.51\ s^{-1}$ and stiffness proportional 1.04×10^{-6} s respectively. were determined experimentally and implemented in the COMSOL model.

In this work, only one set of Rayleigh damping coefficients—are used in the COMSOL Multiphysics simulations. This is appropriate because the study focuses on a single cantilever geometry with fixed material and dimensional parameters. Rayleigh damping depends on the structural properties of the system [20], so these coefficients are specific to the geometry analyzed. For different geometrical configurations or material setups, new values would need to be calculated, as the damping behavior would change accordingly.

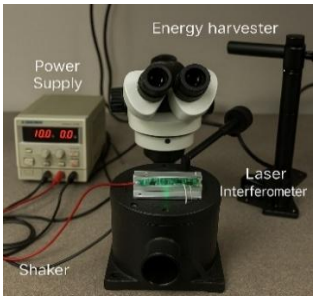

Fig. A-3. Actual Experiment setup.

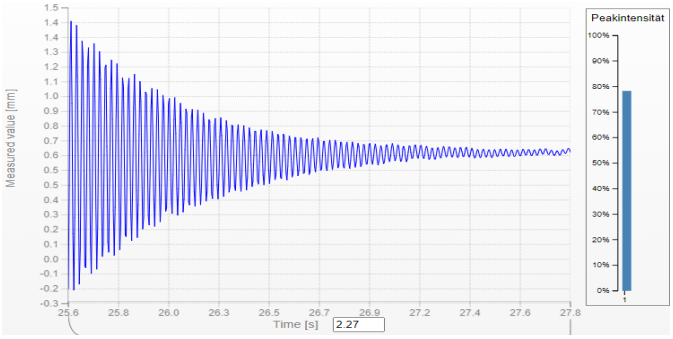

Fig. A-4. Screenshot of damped signal of harvester energy measured by an Interferometer.